Dopaminergic modulation of brain signal variability and the functional connectome during cognitive performance

Mohsen Alavash[1,2+*], Sung-Joo Lim[1,2+],

Christiane Thiel[3], Bernhard Sehm[2], Lorenz Deserno[2],

and Jonas Obleser[1,2*]

[1]Department of Psychology, University of Lübeck, Germany

[2]Max Planck Institute for Human Cognitive and Brain Sciences, Leipzig, Germany

[3]Biological Psychology Lab, Department of Psychology, Carl von Ossietzky Universität Oldenburg, Germany

[+] *M.A. and S.J.L. contributed equally to this work.*

Keywords L-dopa, signal variability, connectivity, graph theory, auditory working memory, fMRI

Abstract

Dopamine underlies important aspects of cognition, and has been suggested to boost cognitive performance. How dopamine modulates the large-scale brain dynamics during cognitive performance has remained elusive, however. Using functional MRI during a working memory task in healthy young human listeners, we investigated the effect of levodopa (L-dopa) on two aspects of brain dynamics, blood oxygen-level-dependent (BOLD) signal variability and the connectome of large-scale cortical networks. We here show that enhanced dopaminergic signaling modulates the two potentially interrelated aspects of large-scale cortical dynamics during cognitive performance, and the degree of these modulations is able to explain inter-individual differences in L-dopa-induced behavioral benefits. Relative to placebo, L-dopa increased BOLD signal variability in task-relevant regions within temporal, inferior frontal, parietal and cingulo-opercular cortices. On the connectome level, L-dopa diminished functional integration in a network of temporo-cingulo-opercular regions. This hypo-integration was expressed as a reduction in network efficiency and modularity, and occurred concurrent with a relative hyper-connectivity in paracentral lobule and precuneus. Both, L-dopa-induced signal variability modulation and functional connectome modulations proved predictive of an individual's L-dopa-induced gain in behavioral measures, namely response speed and perceptual sensitivity. Lastly, signal variability modulation correlated positively with modulation of nodal connectivity and network efficiency in distributed cortical regions. In sum, by providing first evidence for a direct link between dopaminergic modulation of brain signal variability and the functional connectome, we conclude that dopamine enhances information-processing capacity in the human cortex during cognitive performance.

[*]***Corresponding author** Mohsen Alavash, Jonas Obleser; Maria-Goeppert-Str. 9a, 23562 Lübeck, Germany mohsen.alavash@uni-luebeck.de; jonas.obleser@uni-luebeck.de

Significance Statement

How does dopamine shape our cognitive performance? Here we develop and test the hypothesis that enhanced levels of dopamine act upon intra- as well as inter-regional dynamics across the human cortex during a challenging working memory task. We find that, relative to placebo, L-dopa increases signal variability in task-relevant cortical regions, diminishes network integration of temporo-cingulo-opercular regions known to be crucial for sustained attention, and induces hyper-connectivity within the functional connectome. Importantly, the degree of theses modulations explained individuals' behavioral benefits from L-dopa. Notably, L-dopa-induced modulation of signal variability positively correlated with that of the functional connectome in distributed cortical regions. Our findings shed light on how dopamine modulates dynamic communication in the human cortex during cognitive performance.

Introduction

Dopaminergic neurotransmission supports cognitive functions, such as flexible updating and stable maintenance of working memory (Goldman-Rakic, 1995; Wang et al., 2004; Vijayraghavan et al., 2007; Cools and D'Esposito, 2011). The midbrain dopaminergic system innervates widespread areas of cortex ranging from sensory to motor and prefrontal regions (e.g., see Jaber et al., 1996; Seger and Miller, 2010; Frank, 2011, for reviews). Thus, changing dopamine (DA) availability may modulate neural communications among widespread cortical regions and, concomitantly, cognitive performance.

Also, optimal cognitive performance is increasingly recognized to hinge on brain dynamics as measured by signal variability (McIntosh et al., 2008; Garrett et al., 2015; Guitart-Masip et al., 2016; see Grady and Garrett, 2014 for a review). Interestingly and relevant to brain dynamics, DA neurotransmission helps maintain the dynamic range of the neural system (Grace, 1995; Venton et al., 2003; Grace, 2016). A lack of DA reduces phasic activity observed in spike patterns (Paladini et al., 2003), and age-related loss of DA neurons reduces variability of hemodynamic brain responses (Garrett et al., 2015; Guitart-Masip et al., 2016). However, enhanced levels of DA are not beneficial in every individual, and can even be detrimental to task performance depending on individuals' baseline DA and cognitive performance (Cools and Robbins, 2004; for a review, see Cools and D'Esposito, 2011). Recently, Garrett et al. (2015) showed that the extent of DA-related behavioral benefits can be predicted by higher signal variability with increased DA levels in older participants. The hypothesis thus needs testing how changing DA availability impacts on cognitive performance via intermittent, inter-individually differing effects onto brain signal as well as network dynamics.

Moreover, as DA seems to underlie brain signal variability and to innervate functionally diverse cortical areas, changing DA availability should influence functional associations among distributed cortical regions (i.e., the "functional connectome") in the human brain (Giessing and Thiel, 2012; Finn et al., 2015; Bell and Shine, 2016; Mill et al., 2017). Brain signal variability has indeed been suggested as a proxy for information-processing capacity within the functional connectome (Stam et al., 2002;

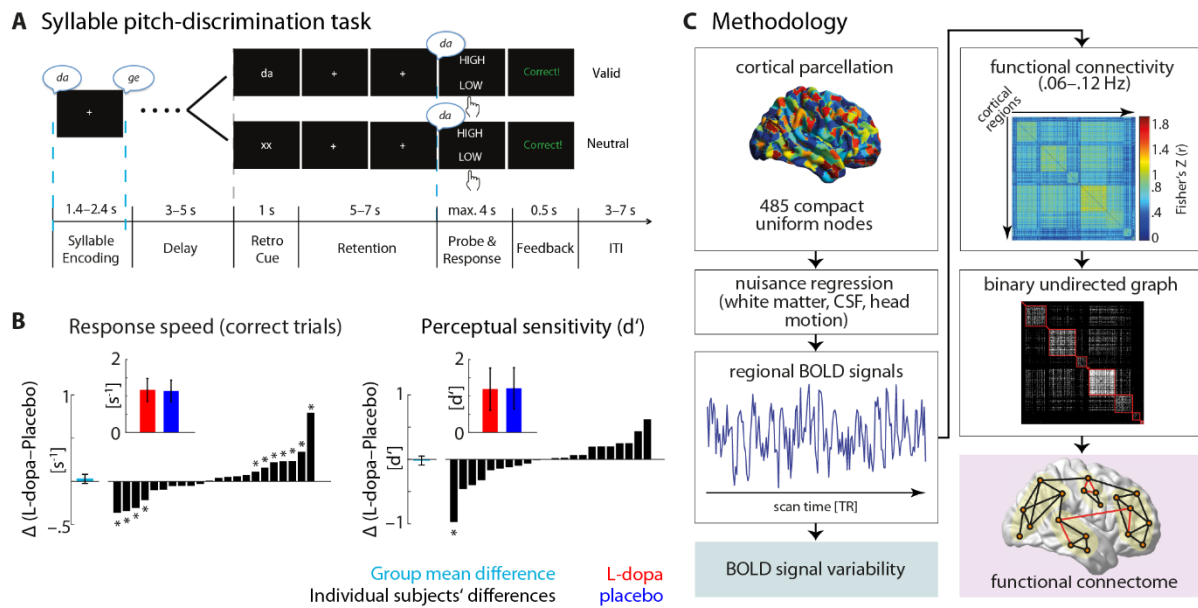*L-dopa modulates large-scale brain dynamics*

Figure 1. Overview of the auditory working memory task, behavioral performances and the methodology used in the study. **(A)** Illustration of a trial structure of the task (adapted from Lim et al., 2015). On each trial participants encoded two auditory syllables and judged whether the pitch of the probe syllable was higher or lower than the same syllable category heard during encoding. Participants received either a valid or neutral retro-cue during the retention period. **(B)** Individuals' and group average behavioral performances in response speed (left) and perceptual sensitivity d' (right). The left most bar (cyan) in each plot represents the group mean difference (Δ: L-dopa–placebo). Error bar: ±1 standard error of the mean (SEM) difference. Asterisk (*): individual subjects (black bars) exhibiting significant behavioral modulations under L-dopa. Inset bars: mean performances (±1 SEM) of the corresponding measures. **(C)** Two analysis streams were used to investigate two aspects of brain dynamics: signal variability and large-scale network topology (see Materials and Methods). Both analyses used mean BOLD signals across voxels within each of 485 parcellated cortical regions. Brain signal variability was computed as the variance of BOLD signal through each fMRI session. The sparse topology of the functional connectome (network density set to 10%) was analyzed using graph-theoretical metrics, which captured functional integration across cortex on local, intermediate and global scales of topology. These include local network efficiency (a metric related to the clustering of a network; red triangle), network modularity (a measure of decomposability of a network into communities; light ovals) and global network efficiency (a metric inversely related to the shortest path between nodes; red path).

McIntosh et al., 2008; Lippe et al., 2009; Mišić et al., 2011; Vakorin et al., 2011; McIntosh et al., 2014). Specifically, higher signal variability has been associated with higher nodal centrality and network efficiency (Mišić et al., 2011), and the difference in signal variability between two cortical nodes has been shown to correlate with the amount of information transferred between them (Vakorin et al., 2011). Accordingly, networks showing higher signal variability have been proposed to have a greater potential for diverse functional configurations (McIntosh et al., 2014) which could have important consequenses for cognitive performance. As of yet, evidence characterizing the impact of DA on the functional connectome is sparse. Achard and Bullmore (2007) demonstrated that a DA antagonist decreased resting-state network efficiency. However, modulation of brain signal variability and the functional connectome may be different during a cognitive task (Nagano-Saito et al., 2008; Mišić et al., 2010; Armbruster-Genç et al., 2016; Cassidy et al., 2016; Rosenberg et al., 2017). Recently, Hernaus et al. (2017) showed that increase of DA and noradrenaline leads to higher fronto-parietal functional connectivity during working memory performance. Nevertheless, it remains unknown how DA

3

modulates large-scale brain network topology during cognitive performance, and how this modulation relates to modulations in brain signal variability and behavior.

In the present fMRI study, young healthy listeners performed an auditory working memory task with and without a single dose (150 mg) of the DA precursor L-dopa. We investigated the effects of L-dopa on blood-oxygen-level dependent (BOLD) signal variability and the functional connectome of large-scale cortical networks, and how such L-dopa-induced modulations relate to modulations in task performance. We used graph-theoretical network analysis to explore the impact of L-dopa on the functional connectivity and integration of large-scale cortical networks engaged during the auditory working memory task. Finally, we examined whether L-dopa-induced modulations in brain signal variability predict L-dopa-induced reorganization of the functional connectome.

Materials and Methods

Participants

Twenty-two healthy young participants (mean age 27.9 years, age range 25–35 years; 12 females) took part in the study. Two additional participants completed the experiment, but were removed from data analysis due to excessive head movements inside the scanner (i.e., total movement > 3.5 mm of translation or degrees of rotation; scan-to-scan movement > 1.5 mm or degrees). Participants reported no histories of neurological or psychiatric disorders, and none were under any chronic medication. Participants were recruited from the Max Planck Institute for Human Cognitive and Brain Sciences database. Prior to participation all volunteers received a separate debriefing session regarding L-dopa by in-house physicians (B.S. and L.D.). All participants gave written informed consent, and were financially compensated (60€ total). All procedures were in accordance with the Declaration of Helsinki and approved by the local ethics committee of the University of Leipzig (EudraCT number 2015-002761-33).

Procedure

All participants underwent two double-blind, counterbalanced fMRI sessions, separated by at least one week. Procedures in both sessions were identical. Each session was completed after administering orally either 150-mg L-dopa (Madopar LT; 150-mg Levodopa/37.5-mg benserazide) or placebo. On each scanning (i.e., medication) session, blood pressure and heart rate were measured four times throughout the experiment: before and after in-take of the pills, and before and after the fMRI scanning. Exclusion criteria were based on physiological changes after medication (i.e., greater than ±20 mm Hg in blood pressure and/or ±10 beats per minute in heart rate); none of the participants were excluded based on these criteria. Before and after pill ingestion, participants completed a questionnaire regarding subjective feelings and physical symptoms (Bond and Lader, 1974). None of the participants were excluded due to side effects of drugs. One participant felt nauseated after the completion of the whole experiment (i.e., including the second fMRI experiment); thus N = 22 data were included in the subsequent analyses.

Approximately 35 minutes after in-take of medication, the fMRI scan started. During this interim period (i.e., prior to scanning), participants completed a short practice session in a separate behavioral testing room to ensure that they understood the main experimental (auditory working memory) task. After the practice session, participants were placed in the scanner and went through a short hearing test of the auditory syllables used in the task with the on-going scanner noise in the background. Time from medication administration to scan onset in minutes was later used as a nuisance regressor in all models reported (see *Statistical analysis*).

We acquired eight functional blocks on each medication session (approximately 50 minutes). During each block, participants completed a total of 16 trials. Behavioral responses were collected via MR-compatible response keys. Participants used both index fingers, each assigned to one of two response keys, to give their response. The mapping between hands and response keys were counterbalanced across participants. All auditory stimulation was presented through MR-Confon headphones (Magdeburg, Germany), with Music safe pro earplugs (Alpine Hearing Protection) providing additional attenuation.

Auditory working memory task

During fMRI acquisition, participants performed a previously established auditory working memory task—a syllable pitch-discrimination task implemented with retroactive cues (see Lim et al., 2015 for more details of the task; Figure 1A). In brief, on each trial participants encoded two distinct auditory syllables (i.e., /da/ and /ge/ presented in a random order), and detected a change in the pitch of one of the syllables after a delay period (jittered between 9–13 s). During the maintenance of the encoded syllables, one of the two types of retro-cue was presented for 1 s on the screen; on equal probability for each task block, a valid cue (written syllable, "da" or "ge") or a neutral cue ("xx") was presented. The valid cue was used to direct participants' attention to one of the to-be-probed auditory syllable. The neutral cue, however, did not provide any information about upcoming auditory probe. After 5–7 s following the visual retro-cue, an auditory probe syllable was presented.

Within a 4-s time window upon hearing the probe, participants compared the pitch of the probe syllable to that of the same category syllable heard during encoding, and responded "high" or "low" accordingly. Syllable pitch change that occurred at probe was parametrically varied in four steps (±0.125 and ±0.75 semitones) relative to its original pitch heard during encoding. On each trial, participants received a visual feedback (written as "correct" or "incorrect" in German) for 500 ms.

Note that we here will not elaborate on effects of cueing on performance or brain dynamics, as we had no hypotheses on how the cueing manipulation should affect our main dependent measures of brain signal and network dynamics.

Syllable tokens were recorded by a native German female speaker. There were 12 different tokens (with varying pitch) for each syllable category, and one token for each category was randomly selected and presented during the encoding phase. The pitch of syllable tokens was manipulated

using Praat (version 5.3). All sound tokens were digitized at 44.1 kHz, had a duration of 200-ms, and normalized to equivalent amplitude (root-mean-squared dB full scale; RMS dBFS).

MRI data acquisition and preprocessing

Whole-brain functional MRI data were collected using a Siemens MAGNETOM Prisma 3T. Functional data were acquired with a 20-channel head/neck coil using an echo-planar image (EPI) sequence [repetition time (TR) = 2000 ms; echo time (TE) = 26 ms; flip angle (FA) = 90°; acquisition matrix = 64 × 64; field of view (FOV) = 192 mm × 192 mm; voxel size = 3 × 3 × 3 mm; inter-slice gap = 0.3 mm]. Each image volume had forty oblique ascending axial slices parallel to the anterior commissure–posterior commissure (AC–PC) line.

Structural images of fifteen participants were available from the database of the Max Planck Institute (Leipzig, Germany), where a magnetization prepared rapid gradient echo (MP-RAGE) sequence had been used to acquire the structural images [TR = 2300 ms; TE = 2.01–2.98 ms; FA = 9°; 1-mm isotropic voxel; 176 sagittal slices]. For participants without pre-existing structural images in the database, a high-resolution T1-weighted structural image was acquired using an MP-RAGE sequence [TR = 2300 ms; TE = 2.98 ms; FA = 9°; 1-mm isotropic voxel; 176 sagittal slices] at the end of the second fMRI session.

Preprocessing. During each functional block 181 volumes were acquired. To allow signal equilibration the first two volumes of each block were removed, and the remaining 179 volumes per block were used for the subsequent analyses. The functional volumes were corrected for slice timing and head motion, and coregistered to each individual's structural image using SPM12 (Frackowiak et al., 2004). The resulting functional volumes were spatially normalized to the standard stereotactic MNI space. No spatial smoothing was applied on the volumes to avoid potential artificial correlations between voxels' BOLD signals, which subsequently constitute the input data for functional connectivity analysis (Figure 1C).

Cortical parcellation. Brain nodes were defined using a parcellated AAL template (Tzourio-Mazoyer et al., 2002) encompassing 485 uniform and compact grey-matter cortical regions (Fornito et al., 2010; Zalesky et al., 2010; Figure 1C). This template was used to estimate the mean BOLD signals across voxels within each cortical region per participant. To minimize the effects of spurious temporal correlations induced by physiological and movement artifacts, a general linear model (GLM) was constructed to regress out white matter and cerebrospinal fluid (CSF) mean time series together with the six rigid-body movement parameters (Hallquist et al., 2013; Jo et al., 2013). Subsequently, the residual time series obtained from this procedure were concatenated across the eight blocks per medication session for each participant. The time series were further processed through two analysis streams (Figure 1C): one analysis focused on BOLD signal variability (univariate approach) and the other on functional connectivity and network topology (multivariate approach).

Brain signal variability

Prior to quantifying signal variability, we equated the mean BOLD signal throughout the experiment blocks for each medication session to remove block-wise drifts (e.g., Garrett et al., 2010, 2011, 2013). To this end, we demeaned the residual BOLD time series such that the signal for each cortical region of each block was at zero. For each region, BOLD signal variability was expressed as the variance of the resulting normalized signal concatenated for each medication session (i.e., 8 blocks). Note that instead of computing the standard deviation of BOLD signal (cf. Garrett et al., 2010, 2011, 2013), the variance was used. This was done to compute actual differences in signal variance while avoiding scaling changes due to the non-linear transformation from variance to standard deviation.

Signal variability for each cortical region represents region-level signal dynamics. Signal variability on the whole-brain level was computed as the mean variance across all cortical regions (i.e., 485 regions). Signal variability was separately quantified for the L-dopa and placebo sessions. L-dopa-induced modulation of signal variability was then quantified as the difference of BOLD signal variability between L-dopa versus placebo (i.e., L-dopa–placebo). As such, we treated the placebo session as baseline for both brain and behavior during the auditory working memory task.

Functional connectivity

First, mean residual time series were band-pass filtered by means of maximum overlap discrete wavelet transform (Daubechies wavelet of length 8; Percival and Walden 2000), and the results of the filtering within the range of 0.06–0.12 Hz (wavelet scale 2) were used for further analyses. It has been previously documented that the behavioral correlates of the functional connectome are best observed by analyzing low-frequency large-scale brain networks (Salvador et al., 2005; Achard et al., 2006; Achard et al., 2008; Giessing et al., 2013; Alavash et al., 2015). The use of wavelet scale 2 was motivated by previous work showing that performance during cognitive tasks predominately correlated with changes in functional connectivity in the same frequency range (Bassett et al., 2010; Alavash et al., 2016). To obtain a measure of association between each pair of cortical regions, Pearson correlations between wavelet coefficients were computed, which resulted in one 485×485 correlation matrix for each participant and medication session (Figure 1C).

Connectome analysis

Brain graphs were constructed from the functional connectivity matrices by including the top 10% of the connections in the graph according to the rank of their correlation strengths (Ginestet et al., 2011; Fornito et al., 2013). This resulted in sparse binary undirected brain graphs at a fixed network density of 10%, and assured that the brain graphs were matched in terms of density across participants and medication sessions (van Wijk et al., 2010; van den Heuvel et al., 2017).

Mean functional connectivity was calculated as the average of the upper-diagonal elements of the sparse connectivity matrix for each participant per medication session. In addition, three key topological metrics were estimated: mean local efficiency, network modularity, and global network

efficiency. These graph-theoretical metrics were used to quantify functional integration of large-scale brain networks on the local, intermediate, and global scales of topology, respectively (Alavash et al., 2017; Figure 1C).

For each topological property, we computed a whole-brain metric, which collapses the measure of network integration into one single value, and a regional metric characterizing the same network property but for each cortical region (Rubinov and Sporns, 2010). The regional network metrics were therefore used to localize cortical regions contributing to the L-dopa-induced modulations observed on the whole-brain level. We used nodal connectivity (also known as 'nodal strength') as the regional measure of mean functional connectivity. Local efficiency was computed within each cortical region's neighborhood graph as the regional measure of mean local efficiency. Finally, nodal efficiency was measured to capture the integration of a given region to the entire network, hence representing the regional measure of global network efficiency (see Figure 1C for an illustration). Below we provide the formalization of the above-mentioned graph-theoretical network metrics.

Nodal connectivity and degree. Nodal connectivity was measured as the average weights of the connections linking a cortical node to the other nodes. Nodal degree (a simple measure of degree centrality) was quantified as the number of connections per node. Fragmented nodes were identified as nodes with a degree of zero, accordingly.

Network dyads. A pair of connected nodes within a graph forms a dyad. A dyad can be comprised of one direct connection (topological distance of one) or several indirect connections, which form paths between two nodes (see Figure 1C). Disconnected dyads can be identified as pairs of nodes with infinite topological distance (unreachable).

Global network efficiency. For a given graph G comprised of N nodes, global efficiency E_{global} summarizes the integrity of the network as 'one whole,' and is estimated by the inverse of the harmonic mean of the shortest path lengths (i.e. the smallest number of intervening connections) between each pair of nodes $L_{i,j}$:

$$E_{global} = \frac{1}{N(N-1)}\sum_{i \neq j \in G}\frac{1}{L_{i,j}} \qquad \text{(Eq.1)}$$

A highly-integrated network is characterized by a short average minimum path length between all pairs of nodes. Such a network is considered to have high efficiency in parallel (or global) information processing (Bullmore and Sporns, 2009). Likewise, nodal efficiency at node i, $E_{nodal(i)}$, (as the regional measure of global network efficiency) is inversely related to the path length of connections between a specific node and the rest of the nodes (Latora and Marchiori, 2001):

$$E_{nodal(i)} = \frac{1}{(N-1)}\sum_{j \in G}\frac{1}{L_{i,j}} \qquad \text{(Eq.2)}$$

Local network efficiency. By slightly zooming out from a given node within a graph, the nearest neighbors of the node that are directly connected to each other form a cluster. This local integration can be quantified based on the local efficiency of node i, $E_{local(i)}$, which is mathematically

equivalent to global efficiency (Eq.1) but is computed on the immediate neighborhood of node i. On the whole-brain level, by averaging local efficiency across all nodes, mean local efficiency can be quantified:

$$E_{local} = \frac{1}{N}\sum_{i \in G} E_{local(i)} \qquad \text{(Eq.3)}$$

Network modularity. Modularity describes the decomposability of a network into non-overlapping sub-networks having relatively dense intra-connections and relatively sparse inter-connections. Rather than an exact computation, modularity of a given network is estimated using optimization algorithms (Lancichinetti and Fortunato, 2009; Steinhaeuser and Chawla, 2010). The extent to which a network partition exhibits a modular organization is measured by a quality function, the so-called *modularity index* (Q). We used a common modularity index originally proposed by Newman (2006), and employed its implementation in the Brain Connectivity Toolbox (Rubinov and Sporns, 2010) which is based on the modularity maximization algorithm known as Louvain (Blondel et al., 2008). The modularity index optimized by this algorithm ranges between 0 and 1, and is defined as:

$$Q = \frac{1}{2W}\sum_{i,j}\left[A_{i,j} - \gamma \frac{k_i k_j}{2W}\right]\delta(c_i, c_j) \qquad \text{(Eq.4)}$$

where $A_{i,j}$ represents the weight (zero or one if binary) of the links between node i and j, $k_i = \sum_j A_{i,j}$ is the sum of the weights of the links connected to node i, and c_i is the community or module to which node i belongs. The δ-function $\delta(u,v)$ is 1 if $u = v$ and 0 otherwise, and $W = \frac{1}{2}\sum_{i,j} A_{i,j}$. Similar to previous work (Bassett et al., 2010; Alavash et al., 2016), the structural resolution parameter γ (see Fortunato and Barthelemy, 2007; Lohse et al., 2014) was set to unity for simplicity. The maximization of the modularity index Q gives a partition of the network into modules such that the total connection weight within modules is as large as possible, relative to a commonly used null model whose total within-module connection weights follows $\frac{k_i k_j}{2W}$. Q is high if a network can be decomposed into modules with many connections within and only few connections between them. Thus, higher Q reflects higher functional segregation on the intermediate level of network topology (Rubinov and Sporns, 2010). Due to stochastic initialization of the greedy optimization, the module detection algorithm was applied 100 times for each brain graph, and the partition that delivered the highest Q value was kept (see Lancichinetti and Fortunato, 2012; Bassett et al., 2013, for other approaches to construct representative high-modularity partitions).

Statistical analysis

Control of medication-session order and other confounding factors. In the present study, all participants went through the same procedure twice on separate days. Consequently, we observed significant effects of session order (first vs. second scan session), regardless of medication conditions, on both behavioral and brain measures. Expectably, participants were significantly faster in the second session ($F_{1,21} = 8.66$; p = 0.008). Also, global network efficiency and network modularity (Q) were significantly higher in the second session (E_{global}: Cohen's d = 0.4, p = 0.008; Q: Cohen's d =

0.43, p = 0.02). This could be arguably due to differences in arousal and/or having easier time in performing the auditory working memory task, as participants are likely to be more relaxed and adapted to drug administration, scan procedure, and task during the second session (Fan et al., 2012; Kitzbichler et al., 2011; Stevens et al., 2012).

To control for potential confounding factors in the interpretation of L-dopa effects, all ensuing comparisons of L-dopa versus placebo were performed on residualized measures, that is, after regressing out covariates of no interest. These covariates included medication-session order (L-dopa first vs. placebo first), body mass index (BMI), and time from medication administration to scan onset.

Behavioral data. For each medication session, we calculated average response speed on correct trials (i.e., an inverse of response time) and a bias-free measure of perceptual sensitivity, d′ (MacMillan and Creelman, 2004). In order to assess the overall effect of L-dopa on behavioral performance across participants, we performed a separate repeated-measures analysis of variance (ANOVA) on response speed and perceptual sensitivity d′. To control for potential confounding factors in the interpretation of L-dopa effects, covariates of no interest (as listed above) were regressed out from the behavioral measures prior to conducting an ANOVA.

To visualize the robustness of L-dopa-induced change in individual participant's performance (Figure 1B), single-subject 95% confidence intervals (CIs) were constructed based on bootstrapped performance differences between L-dopa and placebo (1,000 replications by resampling single-subject trials per session). For a given behavioral measure, a significant change under L-dopa (versus placebo) per participant was inferred if the bootstrapped 95% CI did not cover zero.

Medication effects on brain measures. On the whole-brain level, statistical comparisons of signal variability and network metrics between L-dopa and placebo sessions were based on exact permutation tests for paired samples. We used Cohen's d for paired samples as the corresponding effect size (Gibbons et al., 1993; Hentschke and Stuttgen, 2011; Lakens, 2013).

On the regional level, and for the analysis of both brain signal variability and network metrics, a bootstrap procedure with 10,000 replications was employed to test the medication effect. The bootstrap procedure allowed us to use a CI-based correction method to account for multiple comparisons across cortical regions (see below). For every cortical region per participant, we first computed the difference between the regional metrics (i.e., L-dopa–placebo). Then, the bootstrap distribution of the mean difference across all participants was estimated and used for statistical inference. Finally, Cohen's d for paired samples was calculated as an effect size (Gibbons et al., 1993; Hentschke and Stuttgen, 2011; Lakens, 2013).

Correlational analyses. We further performed correlation analyses to examine whether the individual magnitude of L-dopa-induced modulations of brain signal variability and networks would relate to the individual magnitude of behavioral modulations. To this end, we computed the L-dopa-induced modulations by taking a difference (i.e., L-dopa–placebo) in both brain and behavioral measures. As such, we treated the placebo session as baseline for both brain and behavior during the auditory working memory task. Consistent with the analysis of behavioral data described above,

we accounted for the potential confounding factors prior to the correlation analyses by regressing out the covariates of no interest (i.e., medication-session order, BMI, time from medication administration to scan onset).

Correlations between L-dopa-induced modulations in brain dynamics (i.e., BOLD signal variability or brain network metrics) and modulations in task performance were tested using rank-based Spearman correlation (rho). On the whole-brain level, the significance of the correlations was tested using a permutation test with 10,000 randomizations (Pesarin and Salmaso, 2010). On the regional level, a bootstrap procedure with 10,000 replications of the correlation coefficients was used for statistical inference. Using the same bootstrap procedures, we further examined the relationship between dopamine-related modulation of BOLD signal variability and modulations of the functional connectome.

Significance thresholds. For all statistical tests, we used $p < 0.05$ (two-sided) as uncorrected threshold of significance. For the regional analysis, and to correct for multiple comparisons entailed by the number of brain regions, we implemented the false coverage-statement rate (FCR) correction method (Benjamini and Yekutieli, 2005; applied e.g. in Obleser et al., 2010; Alavash et al., 2017). This method first selects the regions where the bootstrap distribution of the mean difference or correlation coefficients do not cover zero at the confidence level of 95%. In a second correction pass, FCR-corrected CIs for these selected regions are (re-)constructed at a level of $q_{FCR} = 1 - F_s \times \frac{q}{F_t}$, where F_s is the number of selected regions at the first pass, and F_t is the total number of brain regions. The tolerated rate for false coverage statements is q, here 0.05, at which the enlarged FCR-corrected intervals thus control the false-positive rate at the desired level.

Results

Effect of L-dopa on behavioral performances

Figure 1B illustrates the effect of medication (i.e., L-dopa vs. placebo) on overall behavioral performances in the auditory working memory task. Expectably and based on previous studies (see Cools and D'Esposito, 2011 for a review), neither of the behavioral performance measures showed a consistent medication effect overall across participants (repeated-measures ANOVA with nuisance variables controlled; main effect of medication on response speed: $F_{1,21} = 0.22$, $p = 0.65$, $\eta^2_p = 0.01$; main effect on perceptual sensitivity d': $F_{1,21} = 0.13$, $p = 0.73$, $\eta^2_p = 0.006$).

There was sizable inter-individual variation in the degree to which behavior benefitted (or suffered) from the L-dopa manipulation. According to single-subject bootstrapped distributions of the L-dopa versus placebo difference, most participants did not exhibit significant detriments or benefits in perceptual sensitivity d' under L-dopa. Response speed showed a similar, if more clear-cut, inter-individual variation, with 7 out of 22 participants exhibiting a significant response speed-up under L-dopa, and 4 out of 22 participants showing significant slowdown (Figure1B). Hence, in

the next sections, we further investigated whether such inter-individual differences can be explained by L-dopa-induced modulations in brain dynamics (cf. Sharot et al., 2012).

Modulation of signal variability under L-dopa vs. placebo

We started by investigating whether L-dopa modulates brain signal variability. We tested BOLD signal variability changes (L-dopa vs. placebo) on the whole-brain (i.e., average signal variability across all regions) as well as regional level. On the whole-brain level, a slight increase in BOLD signal variability with L-dopa relative to placebo was observed, but this increase was not statistically significant ($M_{L-dopa-Placebo}$ = 1.33; Cohen's d = 0.24; p = 0.30).

Next, we continued by analyzing signal variability on the regional level. L-dopa-induced modulations of signal variability were evident and statistically significant across a distributed set of sensory as well as heteromodal cortical regions. As illustrated in Figure 2A, we observed increased BOLD signal variability under L-dopa in bilateral superior temporal cortices extending from anterior to posterior portions, in bilateral inferior frontal gyri (IFG), and in right supramarginal gyrus (SMG). Also, L-dopa increased signal variability in visual cortical regions including bilateral fusiform gyri. In addition, an L-dopa-induced increase of signal variability was observed in the cingulate cortex, bilateral motor cortices in the pre- and post-central regions, and the right temporo-parietal junction. Except for one region in the left middle frontal gyrus exhibiting a decrease in variability under L-dopa (Cohen's d = 0.31), our results demonstrate that a distributed set of cortical regions relevant for the task increases its signal variability under L-dopa.

Subsequently, we investigated whether the extent of L-dopa-driven modulations in brain signal variability was predictive of individuals' behavioral benefits from L-dopa. For each region, we evaluated the predictive relationship based on 10,000 bootstrapped iterations of correlation (i.e., Spearman's rho) between modulations of BOLD signal variability and modulations of behavioral performance under L-dopa (i.e., L-dopa–placebo).

With respect to response speed, individuals' BOLD signal variability modulations under L-dopa predicted their gain in response speed under L-dopa. Specifically, greater signal variability in right IFG, bilateral precentral regions, bilateral angular gyri/SMG, and left parietal regions, predicted faster responses under L-dopa (Figure 2B, left). The opposite pattern (i.e., lower variability predicting higher response speed gain under L-dopa) was only observed in the subgenual anterior cingulate cortex.

With respect to perceptual sensitivity, the degree of brain signal variability modulation also correlated positively with L-dopa-induced change in d'—especially so in the left insula, bilateral superior temporal pole, and left parahippocampus (Figure 2B, right). Conversely, signal variability modulations in left postcentral/motor cortical regions exhibited significant negative correlations with d' change.

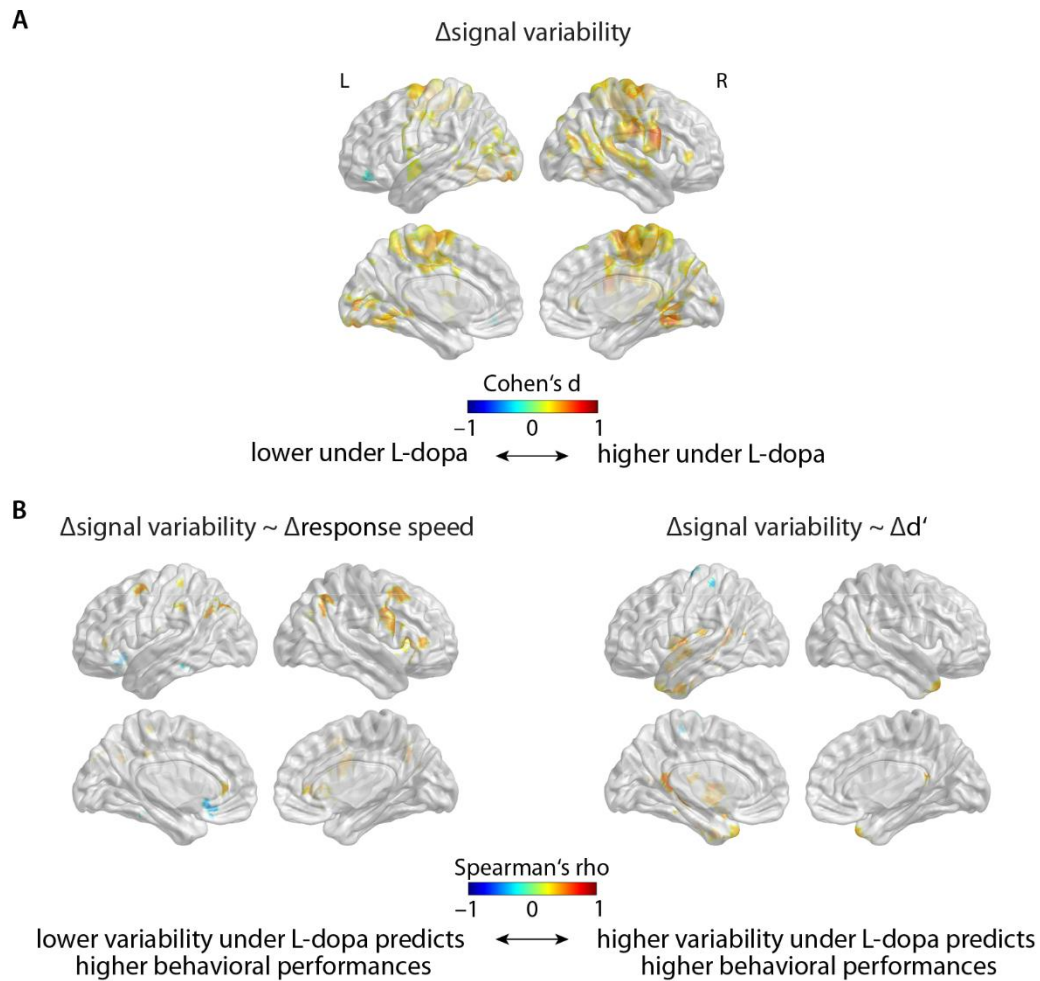*L-dopa modulates large-scale brain dynamics*

Figure 2. L-dopa-related modulation of BOLD signal variability and its relation to modulations of behavioral performance. **(A)** Cortical regions exhibiting significant change in signal variability under L-dopa versus placebo. The difference in signal variability (i.e., Δ: L-dopa–placebo) was expressed as Cohen's d effect size. **(B)** Cortical regions exhibiting significant correlations between L-dopa-induced modulations of signal variability and behavioral performance. Response speed (left) and perceptual sensitivity d' (right). Statistical significance (corrected for multiple comparisons) was ensured based on non-zero coverage of FCR-corrected 95% CIs of the 10,000 replications of bootstrapped distribution of the respective measures in (A) and (B) for each region (see Materials and Methods). Visualizations on the cortical surface were rendered using BrainNetViewer (Xia et al., 2013). L: left; R: right.

Whole-brain modulation of the functional connectome under L-dopa vs. placebo

One of the aims of the present study is to answer how dopaminergic modulation impacts the brain network dynamics engaged in a cognitive task. We approached this question by measuring functional connectivity and integration of large-scale cortical networks using graph-theoretical analysis while participants performed the auditory working memory task separately under L-dopa and placebo. We compared the brain network metrics between L-dopa and placebo across participants. This comparison revealed significant modulations in the connectivity and topology of brain networks under L-dopa versus placebo (Figure 3).

First, functional connectivity showed a significant increase—that is, a relative 'hyper-connectivity'—under L-dopa as compared to placebo (Cohen's d = 0.4, p = 0.03; Figure 3A, top left). Second, functional integration of brain networks showed a significant decrease under L-dopa versus placebo. This relative 'hypo-integration' of brain networks was consistently observed on the local, intermediate and global scales of topology. More specifically, local efficiency of brain networks—a measure inversely related to the topological distance between network nodes within local cliques or clusters—was significantly lower under L-dopa than placebo (Cohen's d = 0.43, p = 0.003; Figure 3A, top right). In addition, modularity of brain networks—grouping of partner nodes within sub-networks—significantly decreased under L-dopa in contrast to placebo (Cohen's d = 0.53, p = 0.002; Figure 3A, bottom left). Moreover, the integrity of brain networks as measured by global network efficiency was significantly lower under L-dopa than placebo (Cohen's d = 0.4, p = 0.012; Figure 3A, bottom right). Thus, L-dopa consistently diminished network integration within the functional connectome on different scales of topology.

Based on these findings, we predicted that L-dopa-induced functional reorganization stems from 'fragmentation' of certain cortical nodes from the entire network. As a disconnection regime, nodal fragmentation can lead to hypo-integration of local clusters, network modules, as well as topologically distant nodes as reflected by a decrease in global network efficiency (Bell and Shine, 2016). Hence, we conducted a more detailed analysis of the functional connectome using two different measures to quantify network fragmentation: the fraction of fragmented nodes (i.e., nodes having no connection, thus having a nodal degree of zero) and the fraction of disconnected dyads (i.e., pairs of nodes that are not reachable from each other). Under L-dopa relative to placebo, brain networks displayed significantly higher fractions of fragmented nodes (Cohen's d = 0.45, p = 0.009; Figure 3B, top) and disconnected dyads (Cohen's d = 0.46, p = 0.007; Figure 3B, bottom).

Next, we investigated whether the reorganization of the functional connectome under L-dopa explains the degree to which participants' behavior gained from L-dopa during the working memory task. We tested the correlation between the modulation (i.e., L-dopa–placebo) in the functional connectome on the one hand, and the modulation in task performance on the other hand. The change in task performance correlated significantly with both, the modulation in functional connectivity and global efficiency of brain networks (Figure 3C). Specifically, participants who showed higher degrees of hyper-connectivity under L-dopa also displayed higher gains in response

L-dopa modulates large-scale brain dynamics

speed under L-dopa than placebo (Figure 3C, left). Besides, participants with lower degrees of global network efficiency (equivalently more pronounced hypo-integration) under L-dopa showed higher perceptual sensitivity (d'; Figure 3C, right). However, the correlation between modulations in mean local efficiency or network modularity (Q) of the functional connectome and either of the performance measures were not significant (E_{local}~response speed: rho = 0.01, p = 0.9; E_{local}~d': rho = –0.23, p = 0.3; Q~response speed: rho = –0.26, p = 0.23; Q~d': rho = 0.19, p = 0.4).

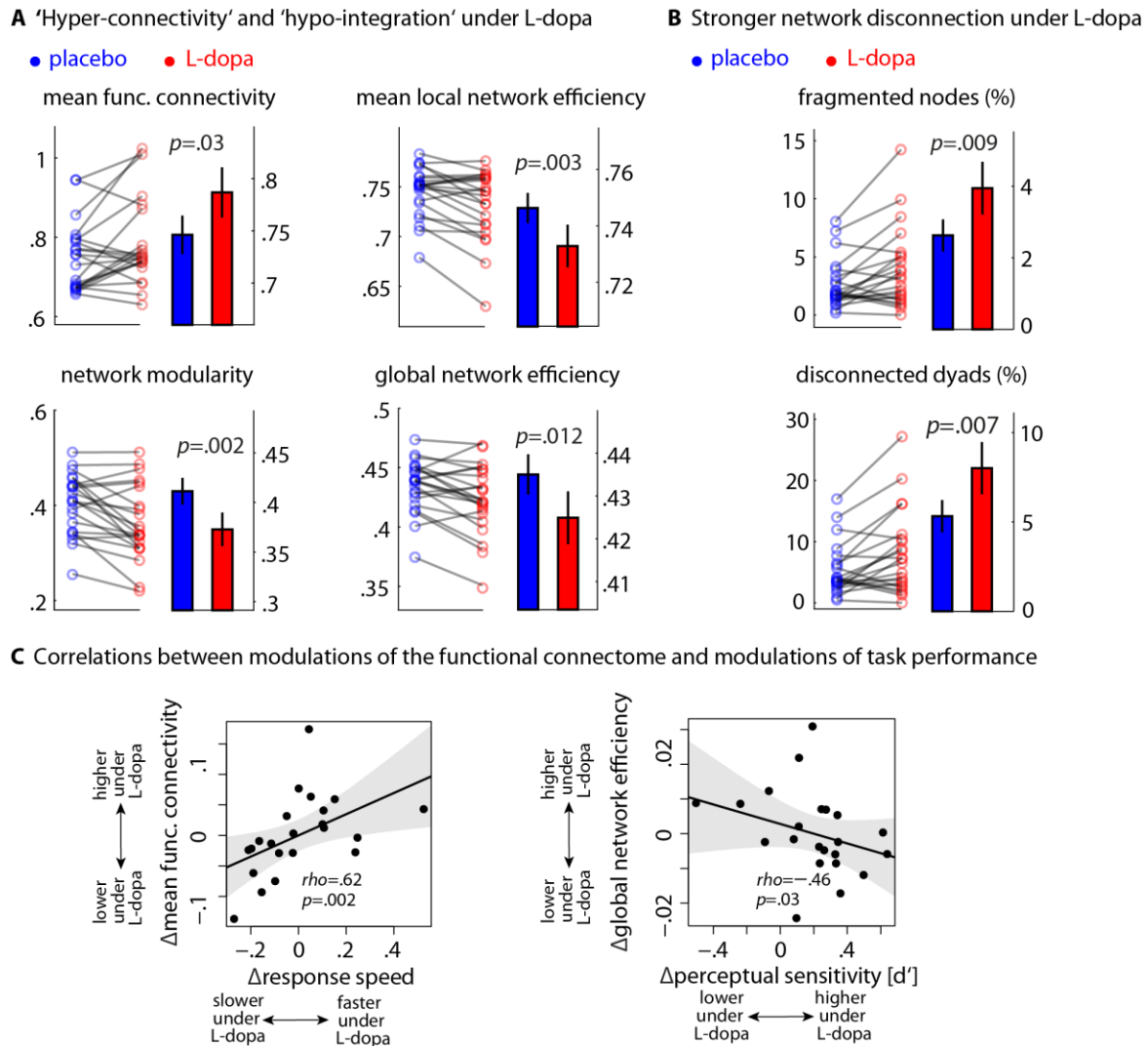*L-dopa modulates large-scale brain dynamics*

Figure 3. Modulation of the functional connectome under L-dopa and its relation to modulations of behavioral performance. **(A)** Whole-brain network metrics under L-dopa and placebo were compared using permutation tests. Circles connected by lines indicate individuals' brain network metrics under placebo and L-dopa. Bar plots show group average brain network metrics (error bars: ±1 SEM). There was a significant increase in functional connectivity—a relative 'hyper-connectivity'—under L-dopa versus placebo. Moreover, functional integration of brain networks showed a significant decrease—a relative 'hypo-integration'—under L-dopa. This pattern was consistently observed for local network efficiency, network modularity and global network efficiency. **(B)** Under L-dopa versus placebo, there were higher proportions of fragmented nodes and disconnected node pairs (dyads). Data are shown using the same illustration scheme as in (A). **(C)** Correlations between modulations of the functional connectome and modulations in behavioral performance (Δ: L-dopa–placebo). Participants who showed higher degrees of hyper-connectivity under L-dopa responded faster. Besides, participants with more pronounced hypo-integration under L-dopa (i.e., lower global network efficiency) showed higher perceptual sensitivity d'. The significance of the Spearman's correlations (rho) was tested using permutation tests with 10,000 randomizations. Shaded area shows two-sided parametric 95% CI. Note that, prior to correlation analysis, all measures were residualized w.r.t. medication session order (L-dopa first versus placebo first), BMI, and time from medication administration to scan onset.

Regional modulation of the functional connectome under L-dopa vs. placebo

To localize cortical regions contributing to the L-dopa-induced modulations observed on the whole-brain level (Figure 3), we analyzed the functional connectome on the regional level. To this end, we used nodal network metrics representing a given network property at each cortical region (see Materials and Methods: *Connectome analysis*). Consistent with the whole-brain level analysis, we compared the regional network properties of the functional connectome between L-dopa versus placebo. We found distributed cortical networks showing significant modulations in their functional connectivity and integration under L-dopa compared to placebo (Figure 4A).

Although these modulations were found in both directions (i.e., L-dopa > placebo and L-dopa < placebo), the most consistent pattern pointed to both hypo-connectivity and hypo-integration under L-dopa within a temporo-cingulo-opercular network (Figure 4A, cold regions). In particular, nodal connectivity and nodal degree of cortical regions mostly in the inferior division of temporal cortex as well as frontal operculum were decreased under L-dopa relative to placebo (Figure 4A, first row). In addition, nodal network efficiency of regions within the inferior portion of temporal cortex, anterior cingulate and frontal operculum was significantly lower under L-dopa than placebo. These findings were further supported by the existence of higher number of fragmented nodes and disconnected dyads in similar regions under L-dopa (versus placebo) within group-average whole-brain networks (Figure 4B).

Next, we tested the correlation between regional modulation (i.e., L-dopa–placebo) of the functional connectome and modulations in behavioral performances. We found significant correlations between modulations of behavioral performances and modulations of nodal connectivity and nodal efficiency (Figure 5). Consistent with the correlations observed on the whole-brain level (Figure 3C), participants who showed increased nodal connectivity (i.e., hyper-connectivity) in bilateral superior temporal/angular gyri and anterior cingulate under L-dopa, also responded faster under L-dopa (Figure 5, left, red circles). Moreover, decreased nodal network efficiency (i.e., hypo-integration) of a brain node within the right frontal operculum/insula under L-dopa predicted higher behavioral gains in perceptual sensitivity (Figure 5, right, blue circle).
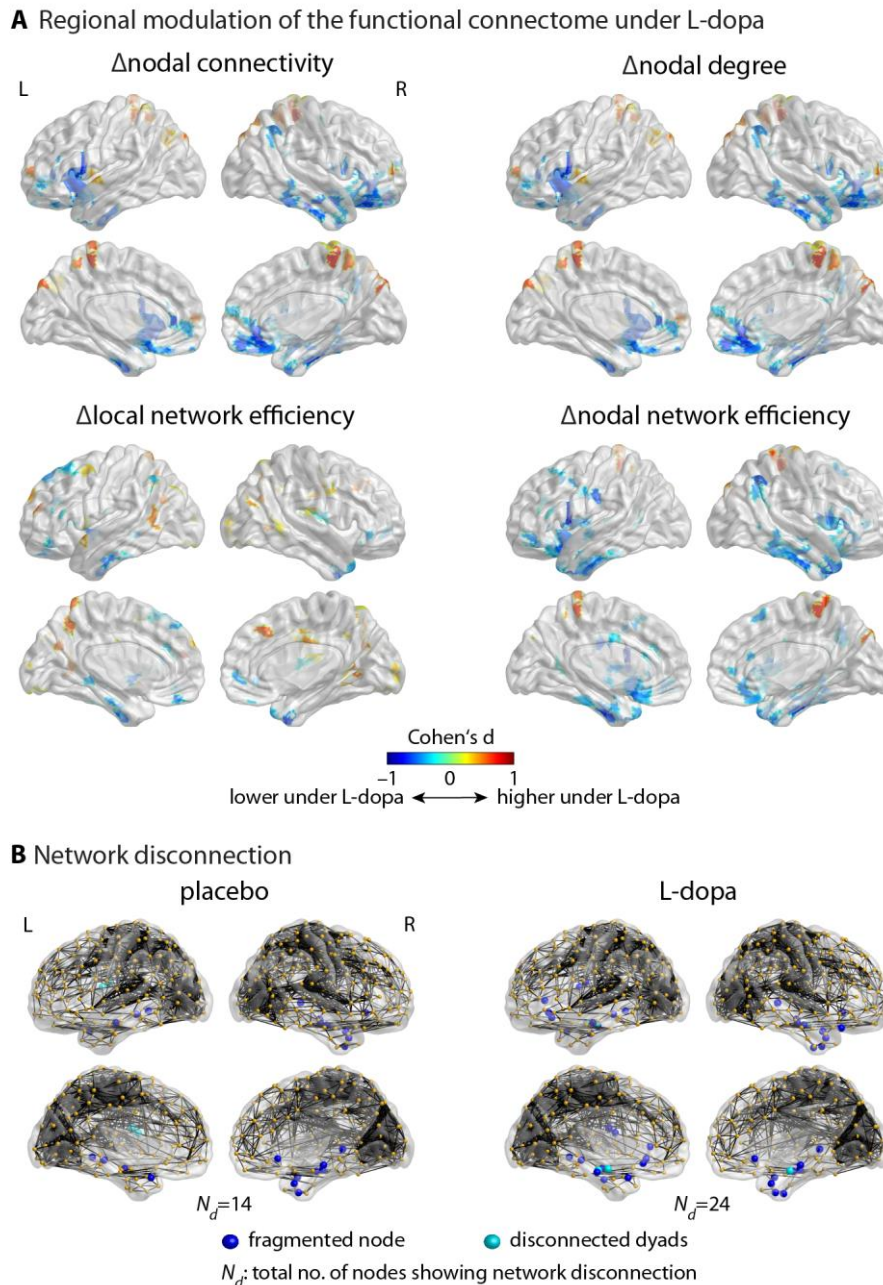
L-dopa modulates large-scale brain dynamics

Figure 4. Cortical regions exhibiting functional connectome modulations under L-dopa. **(A)** Nodal network metrics of cortical regions were compared between L-dopa and placebo using bootstrap procedures with 10,000 replications of group average differences (Δ:L-dopa–placebo). The significance of the differences was inferred based on the FCR-correction method accounting for multiple comparisons. Functional connectivity and network integration were significantly increased (warm colors) or decreased (cold colors) under L-dopa in contrast to placebo, with predominant hypo-integration of temporo-cingulo-opercular regions. **(B)** Network disconnection within the functional connectome. Fragmented nodes and disconnected dyads (unreachable node pairs) were identified based on nodal degree and topological distance between every pair of nodes, respectively. Under L-dopa, the functional connectome displayed higher number of fragmented nodes and disconnected dyads in contrast to placebo (cf. Figure 3B). Group-average networks were constructed by thresholding the mean functional connectivity maps (network density set to 5% for better visualization). L: left, R: right.
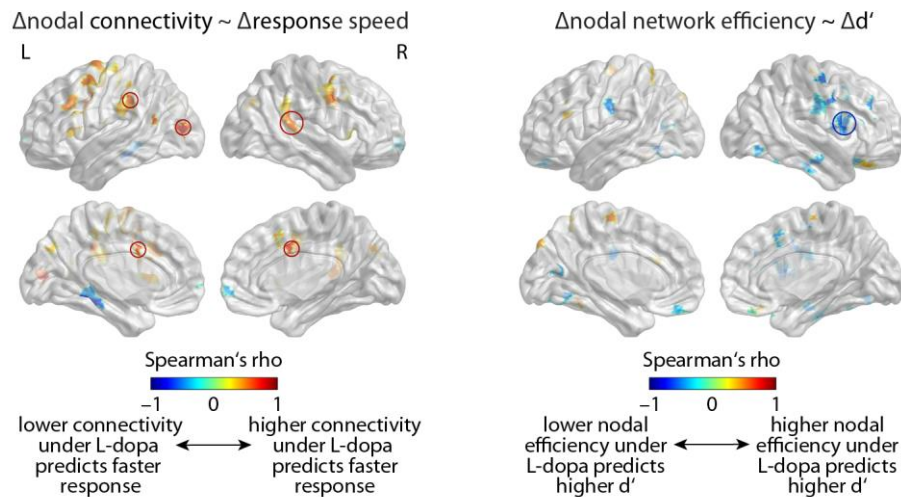
18

Figure 5. Cortical regions where modulation of the functional connectome correlated with modulations in task performance. Modulation of nodal connectivity in bilateral superior temporal/angular gyri and anterior cingulate (left panel, red circles) under L-dopa positively correlated with the change in response speed during the auditory working memory task (Δ:L-dopa–placebo). Additionally, lower nodal network efficiency of a brain node within the right frontal operculum/insula (right panel, blue circle) under L-dopa predicted higher perceptual sensitivity d′. The correlation at each region was tested using a bootstrap procedure for Spearman's rho (10,000 replications). Circles highlight the regions that survived FCR correction (p < 0.05). Colored regions without circles are visualized at the uncorrected level. L: left; R: right.

Relationship of modulations in signal variability and modulations in the functional connectome

Given that L-dopa significantly modulated brain signal variability and network organization of the functional connectome, we further investigated whether these modulations in brain dynamics directly relate to each other across participants. Specifically, we examined which cortical regions exhibit a relationship between the modulation of their signal variability under L-dopa (versus placebo) and the modulation in their network configuration within the functional connectome under L-dopa (versus placebo). We thus separately analyzed the correlations between the modulations of three regional network metrics (i.e., nodal connectivity, local network efficiency, and nodal network efficiency) and modulation in signal variability across cortical regions.

Figure 6 illustrates cortical regions exhibiting robust correlations between modulations in BOLD signal variability and regional network metrics under L-dopa (versus placebo). Across participants, we found that the extent of L-dopa-induced changes in BOLD signal variability positively correlated with the extent of nodal connectivity changes in broadly distributed cortical regions, spanning temporal, cingulate, frontal, and parietal cortices (Figure 6, top).

Interestingly, L-dopa-related modulation of BOLD signal variability predicted the extent of modulation in individuals' brain network efficiency, both on local and global scales of topology. Specifically, network efficiency within each node's neighborhood graph (i.e., local efficiency) as well as its functional integration to the whole-brain graph (i.e., nodal efficiency) significantly correlated with BOLD signal variability in distributed cortical regions. Increased signal variability specifically in temporal, left inferior frontal, cingulate, as well as insula cortices predicted higher network efficiency in similar regions (Figure 6, bottom). Notable exceptions were visual areas (within the occipital and

inferior temporal cortices), which showed negative correlations between modulations in BOLD signal variability and network efficiency.
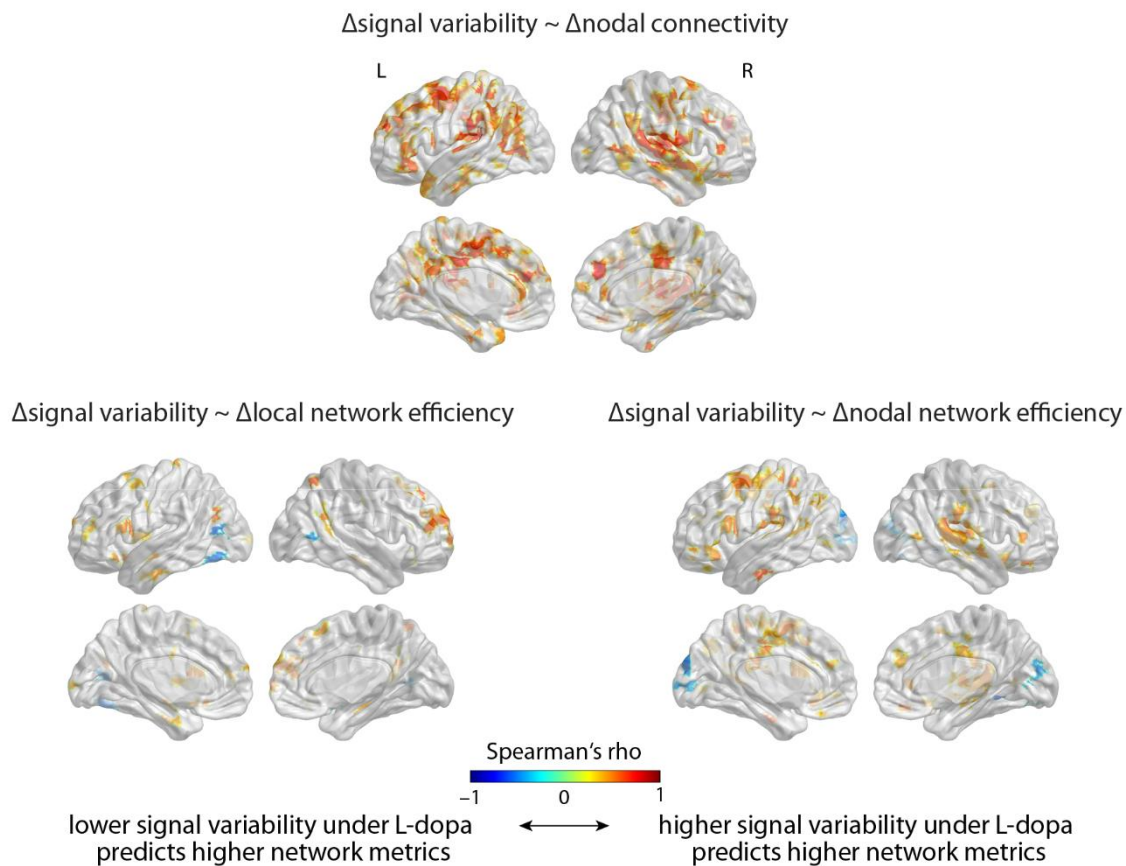

Figure 6. Cortical regions exhibiting significant correlations between the respective modulations of brain signal variability and the functional connectome under L-dopa. The extent of L-dopa-induced modulation of signal variability showed predominantly positive correlations to that of nodal connectivity (top), local network efficiency (bottom, left) and nodal network efficiency (bottom, right) across participants. Δ:L-dopa–placebo. L: left, R: right.

Discussion

How does dopamine modulate the brain dynamics during cognitive performance? We addressed this question by investigating the effect of L-dopa on brain signal variability and the functional connectome while young adults performed an auditory working memory task. We examined L-dopa-induced modulations of brain dynamics and behavior relative to placebo, and the relationships between these modulations.

L-dopa increases brain signal variability

In our sample, L-dopa generally increased brain signal variability. Notably, the individual extent of this increase predicted the behavioral benefit from L-dopa. Our findings are consistent with recent studies emphasizing the importance of signal variability in predicting well-functioning cognitive

L-dopa modulates large-scale brain dynamics

operations (Garrett et al., 2010; Grady and Garrett, 2014), and the role of DA in boosting BOLD signal variability (Garrett et al., 2015).

Specifically, we found that L-dopa increased signal variability in distributed cortical regions deemed relevant for the auditory working memory task. These regions include bilateral superior temporal cortices, often associated with auditory and speech perception (Liebenthal et al., 2005; Obleser and Eisner, 2009). A similar effect was also observed in the bilateral IFG and right SMG, regions implicated in pitch and verbal working memory (Gaab et al., 2003; Obleser and Eisner, 2009). Additionally, L-dopa increased signal variability in domain-general networks overlapping with fronto-parietal and cingulo-opercular regions putatively associated with task control (Dosenbach et al., 2007).

Interestingly, distinct cortical regions appeared relevant in explaining individuals' behavioral benefits from L-dopa. Our results show that loci of signal variability modulations that predict response speed versus d' gains are indeed different. Signal variability in motor and parietal regions seems to underlie response speed gain, whereas L-dopa-induced sensitivity benefits were associated with signal variability changes in parahippocampal area, where activity is related to episodic memory/encoding (Amaral and Insausti, 1990; Davachi et al., 2003; Chowdhury et al., 2012). As we have not observed speed–accuracy trade-offs with the benefits from L-dopa (p = 0.90), it is a tenable hypothesis that signal variability in distinct cortical regions contributes complementarily to behavioral performance.

Dopaminergic neurotransmission is essential in maintaining neural signal dynamics by balancing phasic and tonic neural activities (Grace, 1995; Venton et al., 2003). Given that highly variable signals convey more information (McIntosh et al., 2008), our findings underline the role of DA in optimizing the dynamic range of neural systems involved in processing task-relevant information.

L-dopa substantially modulates the functional connectome

During the auditory working memory task, L-dopa reduced the functional integration of temporo-cingulo-opercular regions. This hypo-integration manifested at different topological scales, and was further supported by a disconnection regime. Since the brain graphs were matched in terms of network density across participants and sessions, this hypo-integration cannot be due to network density differences (cf. van den Heuvel et al., 2017). Given that hypo-integration was dominantly observed in nodal degree and network efficiency of temporo-cingulo-opercular regions, this reorganization most likely stems from a functional disintegration of these nodes from regions less relevant for the task (arguably the default mode network; see Guitart-Masip et al., 2016).

Interestingly, the above hypo-integration correlated with L-dopa-induced sensitivity benefits: participants with more pronounced hypo-integration on both whole-brain and regional levels (right frontal operculum/insula) showed higher d'. These correlations were specific to network efficiency—

a measure related to topological distances, which further supports the functional disintegration of task-relevant regions.

Accordingly, L-dopa-induced hypo-integration might indicate a functional shift of the temporo-cingulo-opercular regions from a globally integrated state to a more autonomous engagement in task processing. Previous work suggests that the cingulo-opercular network is crucial for sustained attention (Dosenbach et al., 2006, 2007; Vaden et al., 2013), hemostatic salience processing (Seeley et al., 2007), and tonic alertness (Sadaghiani and D'Esposito, 2015). Thus, the more autonomous state of this network can increase the signal-to-noise ratio in cortical information processing, and help maintain to-be-attended (here, syllable pitch) information.

To date, only few studies have investigated the effect of DA on brain networks, mostly focusing on resting-state or fronto-striatal functional connectivity (Nagano-Saito et al., 2008; Kelly et al., 2009; Cole et al., 2013; Bell et al., 2015). Our study, in contrast, focuses on large-scale cortical interactions during a listening task with attention and memory components. On the whole-brain level, we found an overall hyper-connectivity under L-dopa. On the regional level, however, we found that L-dopa decreased nodal connectivity of temporo-cingulo-opercular regions, whereas it increased nodal connectivity of paracentral lobule and precuneus. This apparent inconsistency between the direction of the global and regional results can be explained by network disconnection. We found that temporo-cingulo-opercular regions were functionally disconnected (Figure 4B; blue nodes) from the remaining of the whole-brain network (Figure 4B; black connections). The connected component includes the paracentral/precuneus nodes, whose significant increase in nodal connectivity contribute to the hyper-connectivity on the whole-brain level. The disconnected nodes, on the other hand, do not contribute to whole-brain functional connectivity simply due to the absence of connections (hypo-connectivity/-integration). Thus, functional connectivity on the whole-brain level remained significantly higher under L-dopa relative to placebo, the extent of which predicted individuals' response speed gains from L-dopa.

Modulation of signal variability correlates with modulations of the functional connectome

DA-driven modulation of signal variability showed significant positive correlations with modulations of nodal connectivity and network efficiency mainly in temporal and anterior cingulate cortices known to be crucial for listening behavior (Langers and Melcher, 2011; Erb et al., 2013). One might associate these findings with the fact that connectivity between two signals, expressed as their correlation, requires a certain amount of variability. However, the present findings more likely reflect a systematic relationship between two measures of brain dynamics. First, our findings point to the correlation between *modulations* (L-dopa versus placebo) in two measures of brain dynamics rather than within-session correlations. Second, regional network metrics are multivariate measures: nodal connectivity is estimated as mean correlation between a region's signal and its node-pairs' signals, and nodal network efficiency is estimated based on topological distances. Thus, correlation between

the modulation in variability of a regional signal and the modulation in the network wiring of the same region is most likely a systematic relation between two measures of brain dynamics.

These findings can be understood in terms of information-processing capacity (McIntosh et al., 2008; McIntosh et al., 2014), and integration of information across the functional connectome (Tononi et al., 1994; Tononi et al., 1998; Sporns, 2003; Stam and van Straaten, 2012). Our findings are consistent with previous studies reporting positive correlations between entropy of resting-state EEG signals and nodal centrality and network efficiency (Mišić et al., 2010, 2011). Nodes conveying more information are characterized by many connections and short/direct paths to the rest of the network, thereby optimally 'relaying' local information across the connectome (see Timme et al., 2016 for a recent evidence based on networks of neural spikes). Thus, our findings suggest that L-dopa-induced higher signal variability facilitates dynamic communication across the functional connectome.

Limitations and future directions

The present study examined how L-dopa modulates cortical dynamics during working memory performance. Previous studies have emphasized the importance of striatal dopamine in working memory (Frank et al., 2001; Cools et al., 2008; Landau et al., 2009; Guitart-Masip et al., 2016), and even observed an opposite effect of signal variability change with aging in cortical versus subcortical structures (e.g., Garrett et al., 2010). Future investigations would be necessary to examine the influence of DA on neocortical versus subcortical signal variability and networks (Bell and Shine, 2016), and their differential contributions to behavior.

Here, we did not observe a main effect of L-dopa on behavioral performance, but a notably high inter-individual variability in benefits from L-dopa. The absence of an overall effect may be due to the well-known inverted U-shaped effect of DA: Individuals' baseline levels of cognitive performance, endogenous DA, and/or genetic variations in dopamine metabolism determine the direction of L-dopa-related benefits/detriments (Goldman-Rakic et al., 2000; Vijayraghavan et al., 2007; Cools and D'Esposito, 2011; Pearson-Fuhrhop et al., 2013).

Lastly, our sample only involved young participants. Garrett et al. (2015) found that, compared to young adults, stronger DA-related signal variability effects were observed in older age group, whose dopaminergic system may be relatively more degenerated. Thus, in the current study the room for improvement with L-dopa might be smaller in contrast to dopaminergic effects reported in aged participants (Landau et al., 2009; Chowdhury et al., 2012; Garrett et al., 2015; Guitart-Masip et al., 2016). Also, more long-term training might be necessary to observe overall benefits with L-dopa in healthy, young individuals (Knecht et al., 2004).

Conclusion

We showed that experimental increase of dopaminergic levels while performing an auditory working memory task modulated brain signal variability and the functional connectome predominantly in temporo-cingulo-opercular regions. Notably, the degree of these modulations predicted inter-individual differences in behavioral benefits from L-dopa. Our study fills a critical gap in knowledge regarding dopaminergic modulation of univariate and multivariate aspects of brain dynamics. By providing first evidence for a direct link between dopaminergic modulation of brain signal variability and the functional connectome, we conclude that dopamine enhances information-processing capacity in the human cortex during cognitive performance

References

Achard S, Bassett DS, Meyer-Lindenberg A, Bullmore E (2008) Fractal connectivity of long-memory networks. Phys Rev E 77.

Achard S, Salvador R, Whitcher B, Suckling J, Bullmore E (2006) A resilient, low-frequency, small-world human brain functional network with highly connected association cortical hubs. J Neurosci 26:63-72.

Achard S, Bullmore E (2007) Efficiency and cost of economical brain functional networks. PLoS Comput Biol 3:e17.

Alavash M, Daube C, Wöstmann M, Brandmeyer A, Obleser J (2017) Large-scale network dynamics of beta-band oscillations underlie auditory perceptual decision-making. Network Neuroscience 1(2). doi:10.11.62/netn_a_00009.

Alavash M, Thiel CM, Giessing C (2016) Dynamic coupling of complex brain networks and dual-task behavior. NeuroImage 129:233-246.

Alavash M, Doebler P, Holling H, Thiel CM, Giessing C (2015) Is functional integration of resting state brain networks an unspecific biomarker for working memory performance? NeuroImage 108:182-193.

Amaral DG, Insausti R (1990) Hippocampal formation. In: The human nervous system. (Paxinos G, ed). San Diego: Academic Press.

Armbruster-Genç DJ, Ueltzhoffer K, Fiebach CJ (2016) Brain signal variability differentially affects cognitive flexibility and cognitive stability. J Neurosci 36:3978-3987.

Bassett DS, Wymbs NF, Porter MA, Mucha PJ, Carlson JM, Grafton ST (2010) Dynamic reconfiguration of human brain networks during learning. PNAS 108:7641-7646.

Bassett DS, Porter MA, Wymbs NF, Grafton ST, Carlson JM, Mucha PJ (2013) Robust detection of dynamic community structure in networks. Chaos 23:013142.

Bell PT, Shine JM (2016) Subcortical contributions to large-scale network communication. Neurosci Biobehav Rev 71:313-322.

L-dopa modulates large-scale brain dynamics

Bell PT, Gilat M, O'Callaghan C, Copland DA, Frank MJ, Lewis SJ, Shine JM (2015) Dopaminergic basis for impairments in functional connectivity across subdivisions of the striatum in Parkinson's disease. Hum Brain Mapp 36:1278-1291.

Benjamini Y, Yekutieli D (2005) False discovery rate–adjusted multiple confidence intervals for selected parameters. JASA 100:71-81.

Blondel S, Guillaume J, Lambiotte R, Lefebvre E (2008) Fast unfolding of communities in large networks. J Stat Mech P10008:6.

Bond A, Lader M (1974) The use of analogue scales in rating subjective feelings. Psychology and Psychotherapy: Theory, Research and Practice 47:211–218.

Bullmore E, Sporns O (2009) Complex brain networks: graph theoretical analysis of structural and functional systems. Nat Rev Neurosci 10:186-198.

Cassidy CM, Van Snellenberg JX, Benavides C, Slifstein M, Wang Z, Moore H, Abi-Dargham A, Horga G (2016) Dynamic connectivity between brain networks supports working memory: Relationships to dopamine release and schizophrenia. J Neurosci 36:4377-4388.

Chowdhury R, Guitart-Masip M, Bunzeck N, Dolan RJ, Düzel E (2012) Dopamine modulates episodic memory persistence in old age. J Neurosci 32:14193-14204.

Cole DM, Oei NY, Soeter RP, Both S, van Gerven JM, Rombouts SA, Beckmann CF (2013) Dopamine-dependent architecture of cortico-subcortical network connectivity. Cereb Cortex 23:1509-1516.

Cools R, D'esposito M (2011) Inverted-U–shaped dopamine actions on human working memory and cognitive control. Biol Psychiatry 69:e113-e125.

Cools R, Gibbs SE, Miyakawa A, Jagust W, D'Esposito M (2008) Working memory capacity predicts dopamine synthesis capacity in the human striatum. J Neurosci 28:1208-1212.

Cools R, Robbins T (2004) Chemistry of the adaptive mind. Philos Trans A Math Phys Eng Sci 362:2871-2888.

Davachi L, Mitchell JP, Wagner AD (2003) Multiple routes to memory: distinct medial temporal lobe processes build item and source memories. PNAS 100:2157-2162.

Dosenbach NU, Visscher KM, Palmer ED, Miezin FM, Wenger KK, Kang HC, Burgund ED, Grimes AL, Schlaggar BL, Petersen SE (2006) A core system for the implementation of task sets. Neuron 50:799-812.

Dosenbach NU, Fair DA, Miezin FM, Cohen AL, Wenger KK, Dosenbach RA, Fox MD, Snyder AZ, Vincent JL, Raichle ME, Schlaggar BL, Petersen SE (2007) Distinct brain networks for adaptive and stable task control in humans. PNAS 104:11073-11078.

Erb J, Henry MJ, Eisner F, Obleser J (2013) The brain dynamics of rapid perceptual adaptation to adverse listening conditions. J Neurosci 33:10688-10697.

Fan J, Xu P, Van Dam NT, Eilam-Stock T, Gu X, Luo YJ, Hof PR (2012) Spontaneous brain activity relates to autonomic arousal. J Neurosci 32:11176-11186.

Finn ES, Shen X, Scheinost D, Rosenberg MD, Huang J, Chun MM, Papademetris X, Constable RT (2015) Functional connectome fingerprinting: identifying individuals using patterns of brain connectivity. Nature Neurosci 18:1664-1671.

Fornito A, Zalesky A, Bullmore ET (2010) Network scaling effects in graph analytic studies of human resting-state FMRI data. Front Sys Neurosci 4:22.

Fornito A, Zalesky A, Breakspear M (2013) Graph analysis of the human connectome: promise, progress, and pitfalls. NeuroImage 80:426-444.

Fortunato S, Barthelemy M (2007) Resolution limit in community detection. PNAS 104:36-41.

L-dopa modulates large-scale brain dynamics

Frank MJ, Loughry B, O'Reilly R (2001) Interactions between frontal cortex and basal ganglia in working memory: a computational model. Cogn Affect Behav Neurosci1:137-160.

Frank MJ (2011) Computational models of motivated action selection in corticostriatal circuits. Curr Opin Neurobiol 21:381-386.

Gaab N, Gaser C, Zaehle T, Jancke L, Schlaug G (2003) Functional anatomy of pitch memory—an fMRI study with sparse temporal sampling. Neuroimage 19:1417-1426.

Garrett DD, Kovacevic N, McIntosh AR, Grady CL (2010) Blood oxygen level-dependent signal variability is more than just noise. J Neurosci 30:4914-4921.

Garrett DD, Kovacevic N, McIntosh AR, Grady CL (2011) The Importance of being variable. J Neurosci 31:4496-4503.

Garrett DD, Kovacevic N, McIntosh AR, Grady CL (2013) The modulation of BOLD variability between cognitive states varies by age and processing speed. Cereb Cortex 23:684-693.

Garrett DD, Nagel IE, Preuschhof C, Burzynska AZ, Marchner J, Wiegert S, Jungehulsing GJ, Nyberg L, Villringer A, Li SC, Heekeren HR, Backman L, Lindenberger U (2015) Amphetamine modulates brain signal variability and working memory in younger and older adults. PNAS 112:7593-7598.

Gibbons RD, Hedeker DR, Davis JM (1993) Estimation of effect size from a series of experiments involving paired comparisons. Journal of Educational Statistics 18:271-279.

Giessing C, Thiel CM (2012) Pro-cognitive drug effects modulate functional brain network organization. Front Behav Neurosci 6:53.

Giessing C, Thiel CM, Alexander-Bloch AF, Patel AX, Bullmore ET (2013) Human brain functional network changes associated with enhanced and impaired attentional task performance. J Neurosci 33:5903-5914.

Ginestet CE, Nichols TE, Bullmore ET, Simmons A (2011) Brain network analysis: separating cost from topology using cost-integration. PloS One 6:e21570.

Goldman-Rakic PS (1995) Cellular basis of working memory. Neuron 14:477-485.

Goldman-Rakic PS, Muly EC III, Williams GV (2000) D1 receptors in prefrontal cells and circuits. Brain Res Rev 31:295-301.

Grace AA (1995) The tonic/phasic model of dopamine system regulation: its relevance for understanding how stimulant abuse can alter basal ganglia function. Drug Alcohol Depend 37:111-129.

Grace AA (2016) Dysregulation of the dopamine system in the pathophysiology of schizophrenia and depression. Nat Rev Neurosci 17:524-532.

Grady CL, Garrett DD (2014) Understanding variability in the BOLD signal and why it matters for aging. Brain Imaging Behav 8:274-283.

Guitart-Masip M, Salami A, Garrett D, Rieckmann A, Lindenberger U, Bäckman L (2016) BOLD variability is related to dopaminergic neurotransmission and cognitive aging. Cereb Cortex 26:2074-2083.

Hallquist MN, Hwang K, Luna B (2013) The nuisance of nuisance regression: spectral misspecification in a common approach to resting-state fMRI preprocessing reintroduces noise and obscures functional connectivity. NeuroImage 82:208-225.

Hernaus D, Casales Santa MM, Offermann JS, Van Amelsvoort T (2017) Noradrenaline transporter blockade increases fronto-parietal functional connectivity relevant for working memory. Eur Neuropsychopharmacol. doi: 10.1016/j.euroneuro.2017.02.004.

L-dopa modulates large-scale brain dynamics

Hentschke H, Stuttgen MC (2011) Computation of measures of effect size for neuroscience data sets. Eur J Neurosci 34:1887-1894.

Jaber M, Robinson SW, Missale C, Caron MG (1996) Dopamine receptors and brain function. Neuropharmacology 35:1503-1519.

Jo HJ, Gotts SJ, Reynolds RC, Bandettini PA, Martin A, Cox RW, Saad ZS (2013) Effective preprocessing procedures virtually eliminate distance-dependent motion artifacts in resting state fMRI. Journal of Applied Mathematics. doi: 10.1155/2013/935154

Kelly C, de Zubicaray G, Di Martino A, Copland DA, Reiss PT, Klein DF, Castellanos FX, Milham MP, McMahon K (2009) L-dopa modulates functional connectivity in striatal cognitive and motor networks: a double-blind placebo-controlled study. J Neurosci 29:7364-7378.

Kitzbichler MG, Henson RN, Smith ML, Nathan PJ, Bullmore ET (2011) Cognitive effort drives workspace configuration of human brain functional networks. J Neurosci 31:8259-8270.

Knecht S, Breitenstein C, Bushuven S, Wailke S, Kamping S, Flöel A, Zwitserlood P, Ringelstein EB (2004) Levodopa: Faster and better word learning in normal humans. Ann Neurol 56:20–26.

Lakens D (2013) Calculating and reporting effect sizes to facilitate cumulative science: a practical primer for t-tests and ANOVAs. Front Psychol 4:863.

Lancichinetti A, Fortunato S (2009) Community detection algorithms: A comparative analysis. Phys Rev E 80.

Lancichinetti A, Fortunato S (2012) Consensus clustering in complex networks. Sci Rep 2:336.

Landau SM, Lal R, O'neil JP, Baker S (2009) Striatal dopamine and working memory. Cereb Cortex 19:445-54.

Langers DR, Melcher JR (2011) Hearing without listening: functional connectivity reveals the engagement of multiple nonauditory networks during basic sound processing. Brain Connect 1:233-244.

Latora V, Marchiori M (2001) Efficient behavior of small-world networks. Physical Review Letters 87.

Liebenthal E, Binder JR, Spitzer SM, Possing ET, Medler DA (2005) Neural substrates of phonemic perception. Cereb Cortex 15:1621-1631.

Lim S-J, Wöstmann M, Obleser J (2015) Selective attention to auditory memory neurally enhances perceptual precision. J Neurosci 35:16094-16104.

Lippe S, Kovacevic N, McIntosh AR (2009) Differential maturation of brain signal complexity in the human auditory and visual system. Front Hum Neurosci 3:48.

Lohse C, Bassett DS, Lim KO, Carlson JM (2014) Resolving anatomical and functional structure in human brain organization: identifying mesoscale organization in weighted network representations. PLoS Comput Biol 10:e1003712.

Macmillan NA, Creelman CD (2004) Detection theory: a user's guide, Ed 2. London: Psychology.

McIntosh AR, Kovacevic N, Itier RJ (2008) Increased brain signal variability accompanies lower behavioral variability in development. PLoS Comput Biol 4:e1000106.

McIntosh AR, Vakorin V, Kovacevic N, Wang H, Diaconescu A, Protzner AB (2014) Spatiotemporal dependency of age-related changes in brain signal variability. Cereb Cortex 24:1806-1817.

Mišić B, Mills T, Taylor MJ, McIntosh AR (2010) Brain noise is task dependent and region specific. J Neurophysiol 104:2667-2676.

Mišić B, Vakorin VA, Paus T, McIntosh AR (2011) Functional embedding predicts the variability of neural activity. Front Syst Neurosci 5:90.

Mill RD, Ito T, Cole MW (2017) From connectome to cognition: The search for mechanism in human functional brain networks. NeuroImage. doi: 10.1016/j.neuroimage.2017.01.060.

L-dopa modulates large-scale brain dynamics

Nagano-Saito A, Leyton M, Monchi O, Goldberg YK, He Y, Dagher A (2008) Dopamine depletion impairs frontostriatal functional connectivity during a set-shifting task. J Neurosci 28:3697-3706.

Newman ME (2006) Finding community structure in networks using the eigenvectors of matrices. Phys Rev: E 74.

Obleser J, Eisner F (2009) Pre-lexical abstraction of speech in the auditory cortex. Trends Cogn Sci 13:14-19.

Obleser J, Leaver AM, Vanmeter J, Rauschecker JP (2010) Segregation of vowels and consonants in human auditory cortex: evidence for distributed hierarchical organization. Front Psychol 1:232.

Paladini CA, Robinson S, Morikawa H, Williams JT, Palmiter RD (2003) Dopamine controls the firing pattern of dopamine neurons via a network feedback mechanism. PNAS 100:2866–2871.

Pearson-Fuhrhop KM, Minton B, Acevedo D, Shahbaba B, Cramer SC (2013) Genetic variation in the human brain dopamine system influences motor learning and its modulation by L-Dopa. PloS one 8:e61197.

Percival DB, Walden AT (2000) Wavelet methods for time series analysis. Cambridge University Press.

Pesarin F, Salmaso L (2010) The permutation testing approach: a review. Statistica 70:481-509.

Rosenberg MD, Finn ES, Scheinost D, Constable RT, Chun MM (2017) Characterizing attention with predictive network models. Trends Cogn Sci. doi: 10.1016/j.tics.2017.01.011

Rubinov M, Sporns O (2010) Complex network measures of brain connectivity: uses and interpretations. NeuroImage 52:1059-1069.

Sadaghiani S, D'Esposito M (2015) Functional characterization of the cingulo-opercular network in the maintenance of tonic alertness. Cereb Cortex 25:2763-2773.

Salvador R, Suckling J, Coleman MR, Pickard JD, Menon D, Bullmore E (2005) Neurophysiological architecture of functional magnetic resonance images of human brain. Cereb Cortex 15:1332-1342.

Seeley WW, Menon V, Schatzberg AF, Keller J, Glover GH, Kenna H, Reiss AL, Greicius MD (2007) Dissociable intrinsic connectivity networks for salience processing and executive control. J Neurosci 27:2349-2356.

Seger CA, Miller EK (2010) Category learning in the brain. Ann Rev Neurosci 33:203-219.

Sharot T, Guitart-Masip M, Korn CW, Chowdhury R, Dolan RJ (2012) How dopamine enhances an optimism bias in humans. Curr Biol 22:1477-1481.

Sporns O (2003) Network analysis, complexity, and brain function. Complexity 8:56-60.

Stam CJ, van Cappellen van Walsum A, Micheloyannis S (2002) Variability of EEG synchronization during a working memory task in healthy subjects. Int J Psychophysiol 46:53-66.

Stam CJ, van Straaten EC (2012) The organization of physiological brain networks. Clinical Neurophysiology 123:1067-1087.

Steinhaeuser K, Chawla NV (2010) Identifying and evaluating community structure in complex networks. Pattern Recognition Letters 31:413-421.

Stevens AA, Tappon SC, Garg A, Fair DA (2012) Functional brain network modularity captures inter- and intra-individual variation in working memory capacity. PloS one 7:e30468.

Timme NM, Ito S, Myroshnychenko M, Nigam S, Shimono M, Yeh FC, Hottowy P, Litke AM, Beggs JM (2016) High-degree neurons feed cortical computations. PLoS Comput Biol 12:e1004858.

Tononi G, Sporns O, Edelman GM (1994) A measure for brain complexitiy: Relating functional segregation and integration in the nervous system. PNAS 91:5033-5037.

Tononi G, Edelman D, Sporns O (1998) Complexity and coherency: integrating information in the brain. Trends Cogn Sci 2:474-484.

L-dopa modulates large-scale brain dynamics

Tzourio-Mazoyer N, Landeau B, Papathanassiou D, Crivello F, Etard O, Delcroix N, Mazoyer B, Joliot M (2002) Automated anatomical labeling of activations in SPM using a macroscopic anatomical parcellation of the MNI MRI single-subject brain. NeuroImage 15:273-289.

Vakorin VA, Mišić B, Krakovska O, McIntosh AR (2011) Empirical and theoretical aspects of generation and transfer of information in a neuromagnetic source network. Front Syst Neurosci 5:96.

Vaden KI, Jr., Kuchinsky SE, Cute SL, Ahlstrom JB, Dubno JR, Eckert MA (2013) The cingulo-opercular network provides word-recognition benefit. J Neurosci 33:18979-18986.

van den Heuvel M, de Lange S, Zalesky A, Seguin C, Yeo T, Schmidt R (2017) Proportional thresholding in resting-state fMRI functional connectivity networks and consequences for patient-control connectome studies: Issues and recommendations. NeuroImage (In press).

van Wijk BCM, Stam CJ, Daffertshofer A (2010) Comparing brain networks of different size and connectivity density using graph theory. PloS One 5:e13701.

Venton BJ, Zhang H, Garris PA, Phillips PEM, Sulzer D, Wightman RM (2003) Real-time decoding of dopamine concentration changes in the caudate-putamen during tonic and phasic firing. J Neurochem 87:1284-1295.

Vijayraghavan S, Wang M, Birnbaum SG, Williams GV, Arnsten AFT (2007) Inverted-U dopamine D1 receptor actions on prefrontal neurons engaged in working memory. Nat Neurosci 10:376-384.

Wang M, Vijayraghavan S, Goldman-Rakic PS (2004) Selective D2 receptor actions on the functional circuitry of working memory. Science 303:853-856.

Xia M, Wang J, He Y (2013) BrainNet Viewer: a network visualization tool for human brain connectomics. PloS One 8:e68910.

Zalesky A, Fornito A, Harding IH, Cocchi L, Yucel M, Pantelis C, Bullmore ET (2010) Whole-brain anatomical networks: does the choice of nodes matter? NeuroImage 50:970-983.